UDC 538.913: 620.22 - 022.53

A.V. Filimonov [1], A.I. Rudskoy [1], A.A. Naberezhnov [1,2], S.B. Vakhrushev [1,2], A.E. Fotiadi [1], E.Yu. Koroleva [1,2], I.V. Golosovsky [3], Yu.A. Kumzerov [1,2], B. Nacke [4]

[1] St. Petersburg State Polytechnical University
29 Politechnicheskaya St., St. Petersburg, 195251, Russia
[2] Ioffe Physical Technical Institute
26 Politechnicheskaya St., St. Petersburg, 194021, Russia
[3] Petersburg Nuclear Physics Institute,
Gatchina, Leningrad District, 188300, Russia
[4] Leibniz University of Hannover, ETP
4 Wilhelm-Busch-Str., 30167 Hannover, Germany

NANOCOMPOSITE MATERIALS ON THE BASE OF DIELECTRIC POROUS MATRICES

А.В. Филимонов, А.И. Рудской, А.А. Набережнов, С.Б. Вахрушев, А.Э. Фотиади, Е.Ю. Королева, И.В. Голосовский, Ю.А. Кумзеров, Б. Наке

НАНОКОМПОЗИТНЫЕ МАТЕРИАЛЫ НА БАЗЕ ДИЭЛЕКТРИЧЕСКИХ ПОРИСТЫХ МАТРИЦ

The correlations between physical properties and structure of various types of nanocomposite magnetic and ferroelectric materials on the basis of natural and artificial porous have been studied by different experimental methods. The temperature evolution of the structure, order parameter and dielectric response are studied as functions of characteristic size of nanoparticles. It is shown the existence of crossover of phase transition (PT) from the first order to the second one for ultra-small ferroelectric and magnetic particles.

NANOCOMPOSITES, POROUS MATRICES, NEUTRON DIFFRACTION, DIELECTRIC RESPONSE.

Рассматривается влияние условий искусственно ограниченной геометрии на макроскопические свойства, кристаллическую структуру и фазовые переходы в нанокомпозитных материалах на основе пористых матриц с нанометровыми каналами, содержащих внедренные сегнетоэлектрические и магнитные материалы. Показано, что для ряда материалов наблюдается изменение рода фазового перехода, температуры перехода в зависимости от размера наночастицы и характера атомных колебаний. Показано, что для ряда нанокомпозитных материалов, содержащих сегнетоэлектрики, наблюдается резкий рост эффективной диэлектрической проницаемости ε в высокотемпературной фазе.

НАНОПОРИСТЫЕ СТРУКТУРЫ, НЕЙТРОННАЯ СПЕКТРОСКОПИЯ, НАНОКОМПОЗИТЫ, ДИЭЛЕКТРИЧЕСКАЯ СПЕКТРОСКОПИЯ.

I. Introduction

The physical properties of nanostructured materials are one of the «hot» points of modern solid state physics, and they are not only of fundamental interest but also of practical importance. Indeed, it is shown that finite-size effects result in drastic changes of physical properties of ultra-dispersed materials. The observed phenomena become especially significant if the characteristic size of the dispersed particles becomes comparable with the correlation length of the order parameter critical fluctuations, and the development of new nanotechnologies stimulates strongly the studies of various nanostructured and ultra-dispersed substances.

The experimental implementation of new effects in the physics of nanostructures relies upon our ability to create new types of structures and devices. Our understanding of material processing in the pursuit of ultra-small structures is steadily advancing. Epitaxial growth and lateral microstructuring techniques have made it possible to create low-dimensional electronic systems with quantum-confined structures, i. e., quantum wells, quantum wires, and quantum dots.

There are other methods of preparation of such dispersed substances, and one of them is intruding materials into artificial or natural porous matrices. Embedding substances into various porous matrices has some advantages in comparison with other methods:

(a) This method gives a possibility to produce nanostructures with a large range of controlled characteristic sizes from ~ 1 to ~300 nm.

(b) It is possible to prepare nanostructures with various geometry and topology: three-dimensional (3D) dendrite and regular structures, 2D film-like structures, 1D nanowires or 0D small nanoparticles.

One can produce nanoparticles of various substances and compounds: metals, ferroelectrics, dielectrics, insulators, semiconductors, superconductors, magnetic materials and so on.

It is possible to prepare a very large amount (up to several cubic centimeters) of nanocomposite materials (NCM) (or materials in a restricted geometry). This permits us to use some experimental methods that require a large amount of nanostructures (for example, neutron scattering, heat capacity measurements etc.).

Such NCM have been extensively studied during the last years, and it is shown that the reduction of physical size from the microscopic scale down to the meso- and nanoscopic scales results in a change of the majority of physical properties of NCM, such as temperature and type of phase transitions (PT) [1–6], dielectric permittivity [7–9], atomic mobility of constituent ions [10–12], liquids flowing in a confined geometry [12, 13] and so on. One of the important aspects of NCM is phase stability as a function of spatial dimension, geometry, topology and the size of nanoparticles. The properties of NCM and, in particular, various types of PT (superconducting [14–16], superfluid [17, 18], melting-freezing [6, 19–24], and other PTs [4, 7, 25–33] in different NCMs) have been extensively studied by calorimetry [19, 21, 32], NMR [23, 33–34], ultrasonic [35] and dielectric [7–9, 25] measurements, Raman [36, 37], X-ray [26, 28, 30, 38] and neutron scattering [4, 6, 11, 39, 40–48], differential thermal analysis [49], etc. It has been shown that NCMs can form either a system of isolated particles [6] or a net of interconnected dendrite clusters [44, 45], and their physical properties differ drastically from those in corresponding bulk samples and strongly depend on different characteristics of porous matrices and embedded substances such as pore size and geometry, wetting ability, surface tension, interaction between NCM and the surface of the host matrix, and so on.

This contribution is a review of properties and structure peculiarities of magnetic and ferroelectric nanocomposite materials created on the basis of various artificial and natural porous matrices such as porous glasses (3D dendrite interconnected net of nanochannels), artificial opals (3D regular net of nanocaverns), chrysotile asbestos (quasi-1D nanowires), MCM-41 and SBA-15.

II. Nanocomposites with Magnetic Ordering

The magnetic nanoparticles are of great interest because of their unique physical properties in terms of practical applications. It is shown that these properties drastically change in the conditions of restricted or confined geometry. These conditions assume:

the number of atoms at the surface of nanoparticles becomes comparable with the total number of atoms;

particle size is comparable with the length of the magnetic and atomic interaction.

Although the integral methods (e. g., Мцss-bauer spectroscopy, SQUID measurements and others) have the higher luminosity and sensibility in contrast with diffraction, the physical interpretation of any experiment is impossible without knowledge of detailed magnetic and atomic structure of nanoparticles. Obviously, similar information can be obtained by the diffraction methods only, because the electronic (or other) microscopy does not provide the proper accuracy and resolution.

As host matrices we have used porous glasses with average pore diameter of 70 ± 3 Å, SBA-15 matrices with channel diameters of 47 − 87 Å and MCM-41 matrices with channel diameters of 24 − 35 Å. MnO, CoO and Fe_2O_3 were synthesized into the matrices by a chemical bath deposition method. Manganese oxide was selected since the magnetic behavior of the bulk had been well studied. This oxide has an antiferromagnetic structure, for which the magnetic and nuclear Bragg reflections are well separated [50, 51]. The magnetic order in bulk MnO occurs by the first order transition at 117 ± 1 K [52], accompanied by a distortion of the cubic structure [51, 53].

A. The Magnetic Order inside and on the Surface of Nanoparticles

1. Reduction of Magnetic Moment

First neutron diffraction experiments with nanoparticles in the condition of «a restricted geometry» had been performed with the classic antiferromagnet MnO embedded into porous glass [4]. Manganese oxide is very suitable for the studies of magnetism in «the restricted geometry». First, the oxide has a simple antiferromagnetic structure, for which the magnetic

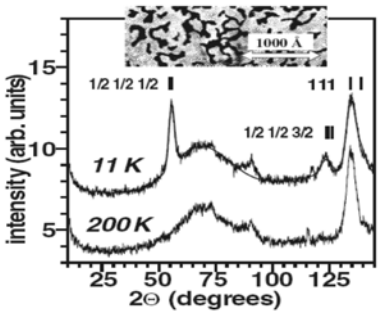

Fig. 1. Neutron diffraction patterns of MnO embedded into a porous glass. The stripes mark the positions of Bragg reflections corresponding to the trigonal distorted lattice. The solid line corresponds to the calculated profile. In the inset the fragment of a typical micrograph of pore network in porous glasses is shown

and nuclear Bragg reflections are well separated. Secondly, MnO is easily synthesized inside the cavities. Thus, it is possible to introduce a large quantity of oxide sufficient to perform neutron research. And thirdly, manganese has a negative nuclear scattering length, while the oxygen has a positive scattering length. This provides a good contrast in the neutron diffraction that allows controlling stoichiometry with high accuracy.

At last, ion Mn^{2+} has a large magnetic moment of 5 μ_B/ion. The magnetic order in the bulk MnO occurs by the first order transition at ~ 117 K, accompanied by a distortion of the cubic structure [53]. Indeed, new Bragg reflections appearing below 122 K (Néel temperature) show the onset of the correlated magnetic order in the embedded nanoparticles (Fig. 1). The diffraction lines are broadened with respect to the instrumental resolution, indicating that the correlation length is finite. The observed diffuse background is due to the porous silica glass. The indexing of the observed magnetic reflections corresponds to antiferromagnetic ordering similar to that for the bulk MnO. The shape of the reflections below the Néel temperature indicates structural distortions and matches to the trigonal distortion of a cubic lattice.

From the intensity of the magnetic Bragg reflections, the ordered magnetic moment at 10 K was found to be 3.84(4) μ_B/ion. This value, averaged over the magnetic region, turns out

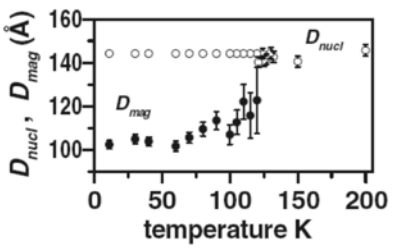

Fig. 2. Temperature dependencies of the volume-averaged diameters of magnetic (D_{mag}) and nuclear (D_{nucl}) regions, solid and open circles respectively

to be noticeably smaller than the experimental value of 4.892 μ_B/ion reported for MnO.

Moreover, the average size of a magnetic cluster turns out to be significantly smaller than the average size of a nanoparticle (Fig. 2). In the diffraction experiment, the surface spins, disordered on atomic scale, do not contribute to the coherent magnetic Bragg reflections. Therefore, the reduction of the net moment can be easily explained by random moment canting. The difference between D_{mag} and D_{nucl} could be due to several factors. It could result from a breakdown of large magnetic aggregates into smaller ones because of the necks or other irregularities in porous media. Another explanation could come from the random canting of spins at the surface of the nanoparticle near the pore walls and the formation of a «layer» with spin disorder. As a result, the orientation of the surface magnetic moments could be altered from that in the core. Such disordering is a well-established phenomenon for nanoparticles.

2. The Electron Spin Resonance (ESR) in MnO

ESR in MnO inside porous media clear shows the existence of the local spin ordering [54]. The analysis of the ESR signal from confined MnO shows two signal components, one of which corresponding to crystallized MnO, while another component is due to MnO in an amorphous state. Such analysis allows us to investigate the magnetic behavior of the crystallized and amorphous parts of the embedded MnO separately.

The ESR signal associated with the crystalline MnO within porous glass shows a behavior having many similarities to the bulk. However, in contrast to the bulk (compare (*a*) and (*c*) panels in Fig. 3), the strong ESR signal due to disordered surface spins is observed below the transition.

3. Magnetic Moments in Different Crystallographic Positions in Maghemite γ-Fe_2O_3

Classical ferrimagnetics, iron oxides, in particular maghemite (γ-Fe_2O_3), are widespread in nature. They have been known since ancient times and are widely applied at present [55]. Neutron diffraction experiments with maghemite show that the oxide, incorporated within porous glass, has the spinel structure with unoccupied positions, which corresponds to the known structure of maghemite [56].

The spinel structure contains two types of voids: tetrahedral (eightfold A position) and octahedral (16-fold B position). Magnetic ions can occupy both positions (Fig. 4). Maghemite has the structural formula

$$(Fe^{3+})[Fe^{3+}_{5/6}\square_{1/6}]_2\{O^{2-}\}_4.$$

In this formula, the parentheses and square brackets refer to the tetrahedral and octahedral voids, respectively, and the symbol □ corresponds to vacancies.

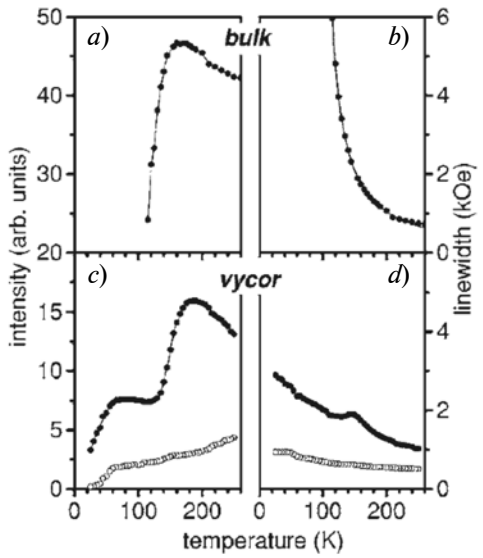

Fig. 3. Intensity (*a*) and lineshape (*b*) of the ESR signal from the bulk MnO. Intensity (*c*) and linewidth (*d*) of the ESR signal from MnO confined to a porous glass.
Open circles correspond to the signal from crystalline MnO and solid circles correspond to the signal from amorphous MnO

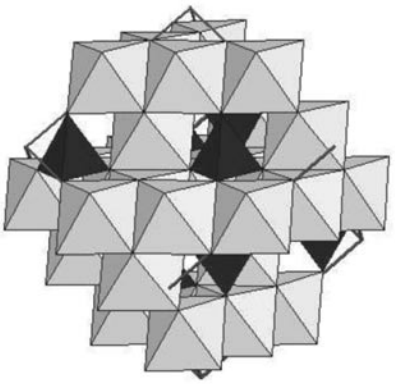

Fig. 4. Crystal structure of spinel with tetrahedral (A) position (in black) and octahedral (B) position (in grey)

It appears that the magnetic moments in confinement are noticeably different in the A and B positions, although Fe^{3+} does not carry any spin moment and crystal field effect should be negligible. Such effect is not observed in the bulk and results from the size-effect.

Let us consider the nearest environment of the magnetic ions at two positions. The magnetic ion in the A position has 4 neighbors in the same positions with the same moment direction and 12 neighbors in the B position with the opposite spin direction. The ion in the octahedral B position has 6 neighbors with the same spin direction in B positions and 6 neighbors with the opposite spin direction in A positions. Assuming the same spin values in the A and B positions, and taking into account the spin directions, the exchange integrals in the A and B positions are proportional to $J_A = -12J_{AB} + 4J_{AA}$ and $J_B = -6J_{BA} + 6J_{BB}$, respectively. Substituting the exchange integral values known for the bulk (we suppose that they are close to those in confinement) maghemite, we obtain $J_A/J_B = 2.19$. Thus, the moment in the B position is bound two times more weakly by the exchange interaction in respect with the A position. The more weakly bound spin in the B position must evidently be more disordered due to the breakings of local symmetry, and, consequently, its mean value is lower.

4. The Coexistence of two Magnetic Phases

This coexistence takes place because of the different constants anisotropy on the surface and in the cores of hematite nanoparticles confined to porous glass [57]. The bulk hematite has the corundum crystal structure and presents two-sublattice antiferromagnet with the Néel temperature of 950 K. At 260 K hematite undergoes a spin-reorientation transition known as the «Morin transition». Below the transition the moments in two magnetic sub-lattices are exactly antiparallel and aligned along the rhombohedral [111] axis (*c*-axis in the hexagonal setting) (AF phase). Above the transition, the moments lie in the basal plane (111) with a slight canting resulting in a weak net moment originating from Dzyaloshinskii – Moriya anisotropic super-exchange interaction (WF phase). The spin flip is related to a competition of two terms with different temperature dependences: the magnetic dipolar interaction and the single-ion anisotropy arising from higher order spin-orbital effects that leads to the different sign of the anisotropy constant.

It turns out that the magnetic contributions into the neutron diffraction patterns from the hematite nanoparticles measured at 300 K and at 10 K are similar. It means that at least down to 10 K there is no any phase transition in confined nanoparticles. In other words, «Morin transition» is suppressed in the «restricted geometry».

Analysis of the observed intensities of the magnetic reflections shows that they substantially differ from the intensities which correspond to the single WF or to the single AF phases. The observed patterns can be equally well described by two models which are indistinguishable in the frame of the neutron powder diffraction.

The first model assumes that the resulting moment tilts from the rhombohedral axis. The alternative model assumes two magnetic phases: in one phase the magnetic moments are aligned along the rhombohedral axis, as in the bulk hematite below the Morin transition (AF phase), and in the other phase the magnetic moments are confined to the perpendicular plane, as in the bulk hematite above the Morin transition (WF phase).

The data analysis of the neutron diffraction taking into account the results of Mössbauer spectroscopy supports the last model of the two co-existing magnetic phases, corresponding to the phases which in the bulk hematite exist

separately above and below the Morin transition. In the case of a nanoparticle, one phase exists at the surface, while another one exists in the core, because of the difference in the anisotropy constants.

B. Magnetic Phase Transitions in the «Restricted Geometry»

1. Continuous Transition in the Nanostructured Nanoparticles

The temperature dependencies of the magnetic moment of the embedded nanoparticles MnO and that in bulk are shown in Fig. 5 [4]. Fitting the observed magnetic moment dependence with the power law

$$m(T) \sim (1 - T/T_N)^{\beta}$$

yields the Néel temperature T_N =122.0(2) in contrast with T_N of 117 K in the bulk.

In Fig. 5 it is clearly seen that the discontinuous, first order transition in the bulk becomes continuous in the «restricted geometry». Rigorously, singularities at phase transitions occur in the thermodynamical limit only, when the system is infinite along some directions in space [58]. If the system is finite along all dimensions, it cannot exhibit a singular behavior. Computer simulation of phase transition in finite-size systems confirms this general idea.

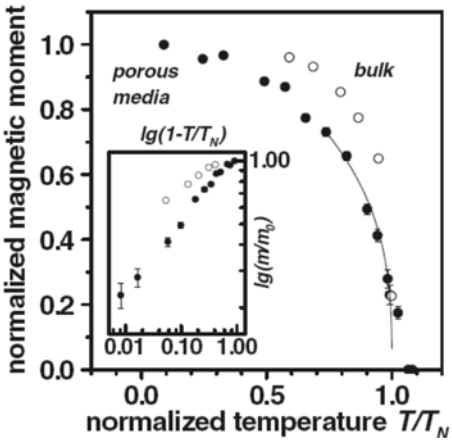

Fig. 5. Temperature dependence of the scaled magnetic moment of MnO embedded in porous glass (solid circles) and of the bulk MnO (open circles). The solid line corresponds to a fit with the power law. The moment dependencies on a logarithmic scale are shown in the inset

There is extensive literature which shows that continuity and «smoothing» («rounding») of the phase transition in the «restricted geometry» is a general phenomenon that comes from the restrictions on the length of the magnetic fluctuations by the size of nanoparticles [59, 60].

Indeed, the correlation length ξ when approaching the transition from the above can be described by a power law:

$$\xi(T) = \xi(0)\left|1 - \frac{T}{T_C(bulk)}\right|^{\nu}.$$

Here ν is so-called critical exponent. In the case of a finite system, the $\xi(T)$ at transition temperature T_C is restricted by the characteristic size of the nanoparticle L:

$$\xi(T_C) = L = \xi(0)\left|1 - \frac{T}{T_C(bulk)}\right|^{\nu}.$$

It immediately follows that T_C in confinement should be lower than the T_C in the bulk:

$$T_C = T_C(bulk)\left[1 - \frac{\xi(0)}{L}\right]^{1/\nu}.$$

Really, this law is observed in all known cases (see, for example, confined CoO [61]). However, the nanostructured compounds with Mn^{2+} ions do not obey this law. Probably, it is connected with the specific electronic structure of Mn^{2+}. Up to now, there has been no clear explanation of this phenomenon.

2. Evolution of the Magnetic Phase Transition in MnO, Nanostructured within the Channels of MCM Matrices

Unusual behavior was observed for nanoparticles of MnO nanostructured within the channels of the MCM-41 matrices in the form of thin nanoribbons. In Fig. 6, the temperature dependencies of the normalized magnetic moment for MnO confined within the channels of different diameter are shown. The solid line corresponds to a fit with the power law

$$m(T) \sim (1 - T/T_N)^{\beta}.$$

Critical exponent β corresponds to the definite theoretical model of the magnetic system. For example, $\beta = 0.5$ corresponds to so-called mean-field theory, when in a three-dimensional system all possible magnetic bonds are working.

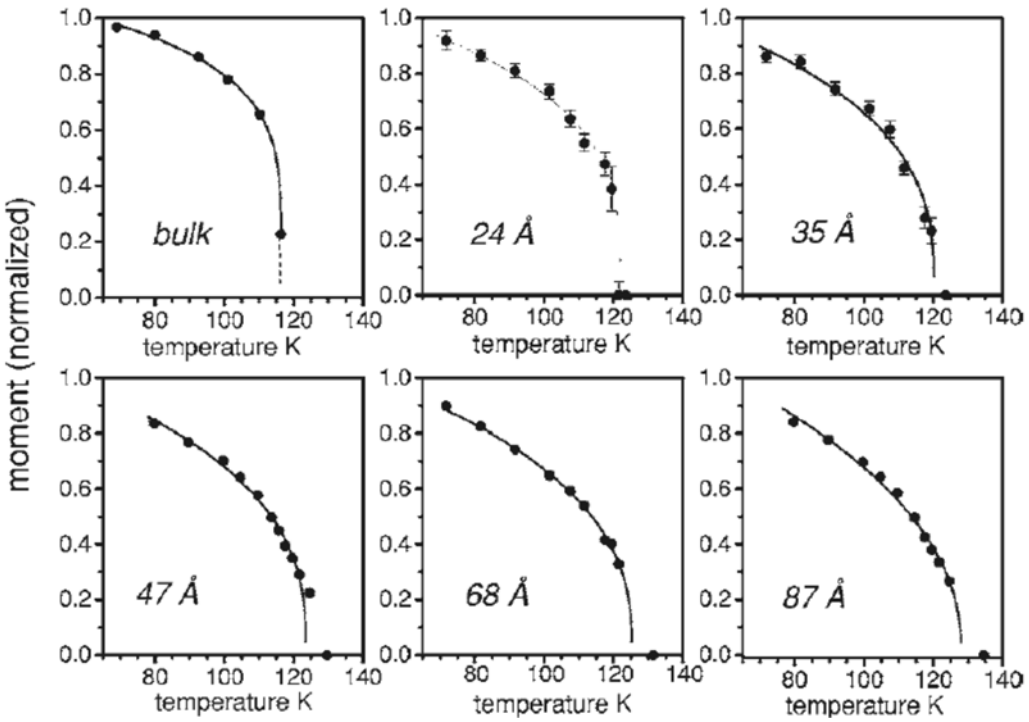

Fig. 6. Temperature dependences of the magnetic moment for MnO confined within the channels of different diameters. The solid lines correspond to a fit with the power law

From neutron and X-ray powder diffraction, it follows that the lengths and thinnesses of the nanoribbons are similar for all matrices. Therefore, the channel diameter is the only characteristic parameter which defines the dimension of the system. In Fig. 7, the channel dependence of the critical exponent β and T_N are shown. It is seen, that with the channel diameter decrease the critical exponent β decreases, and this corresponds to a decrease of the dimensionality of the magnetic system. In other words, with the channel decrease the system anisotropy increases and magnetic system of a nanoparticle becomes more and more close to the one-dimensional model.

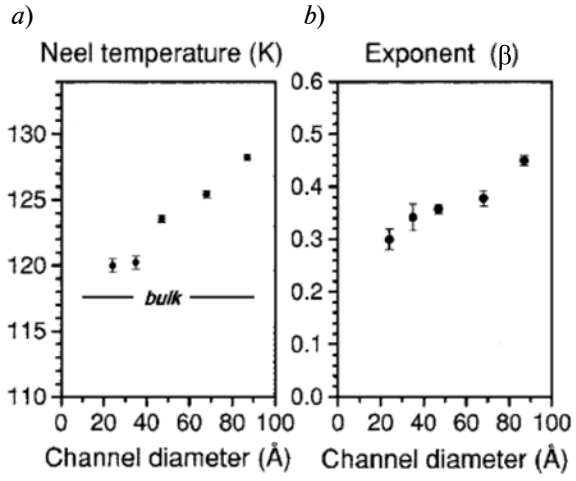

Fig. 7. Dependencies of the Néel temperature T_N (*a*) and exponent β (*b*) on channel diameters from the fitting with the power law

Nanoparticles confined within large channels are expected to behave as constrained three-dimensional systems. However, with a decreasing channel diameter, one expects a crossover with one-dimensional behavior. In this case, the magnetic fluctuations should destroy the long-range magnetic order, and T_N should go to zero. However, in our case we see that T_N does not extrapolate to zero with the decreasing channel diameter (Fig. 6).

C. «Exchange Biased» Magnetic Moment in the «Core-Shell» Systems

Such systems present the antiferromagnetic core of MnO with a thin layer of ferrimagnetic γ-Mn_2O_3 [62, 63]. Remarkably, while the MnO

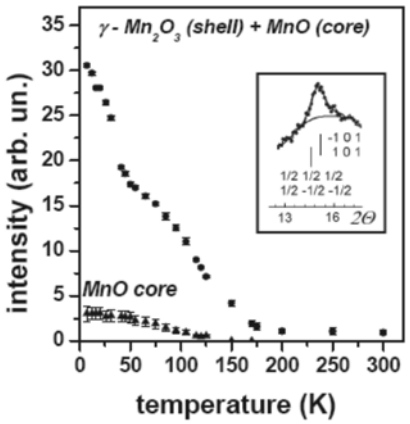

Fig. 8. Temperature dependence of the intensity of the magnetic peak (shown in the insert) with the next contributions from the MnO core: reflections (1/2, 1/2, 1/2), (1/2, −1/2, −1/2) and from the γ-Mn_2O_3 shell: reflections (1, 0, 1) and (−1, 0, 1). The contribution from the MnO core calculated from the profile analysis is shown by triangles

core is found to have a T_N not far from its bulk value (117 K), the magnetic order of the ferrimagnetic shell persists far above T_C (43 K) of the bulk. In Fig. 8, the temperature evolution of the characteristic magnetic reflection is displayed.

It is clearly seen that the magnetic signal, which is proportional to the square of the ferrimagnetic moment observed above T_N and T_C, grows up to the room temperature.

We attribute the observed stable magnetic moment in the ferrimagnetic γ-Mn_2O_3 shell to the exchange coupling between the antiferromagnetic MnO core and the ferrimagnetic shell, as it has been observed in the film layered systems. This phenomenon should be considered as a proximity effect, when the net ferromagnetic moment due to the local violation at the surface (interface) of antiferromagnetic core biases the ferrimagnetic constituent.

III. Ferroelectrics in a Restricted Geometry

For NCM with embedded ferroelectrics, very interesting and sometimes surprising results have been obtained during the last years. In particular, the dielectric measurements of $NaNO_2$, KH_2PO_4 (KDP), KD_2PO_4 (DKDP), Roshelle salt, KNO_3 within porous glasses and artificial opals have shown the unexpected growth of the real and imaginary parts of the dielectric susceptibility ε above the temperature T_C of the ferroelectric PT [7–9, 27, 44, 64]. In such a situation, the increase of the imaginary part of ε could be attributed to the appearance of conductivity, but in this case the microscopic origin of such conductivity was absolutely unclear. The most remarkable result was the giant growth of ε (up to 10^8 at 100 Hz) upon approaching the bulk melting temperature that was observed for $NaNO_2$ embedded in artificial opals.

These experimental results were the starting point for a detailed study of the temperature evolution of structure of confined $NaNO_2$. To understand the microscopic nature of observed giant growth of dielectric permittivity in paraelectric phase, we have performed the complex study of the structure and properties of these NCM including neutron scattering, measurements of heat capacity, NMR, small angle neutron scattering (SANS), dielectric measurements, etc.

A. Samples

Sodium nitrite belongs to order-disorder ferroelectrics and undergoes the first order phase transition at $T_C \approx 437$ K. At room temperature (RT), $NaNO_2$ has a body centered orthorhombic lattice ($a = 3.57$ Å, $b = 5.578$ Å, $c = 5.39$ Å) with two molecules per unit cell, and its space group is *Im*2*m*. In the low-temperature ferroelectric phase, the spontaneous polarization points along the *b*-axis and appears due to a partial alignment of NO_2 groups along this axis, accompanied by the displacement of sodium ions. At high temperature (above T_C), a mirror plane perpendicular to the *b*-axis appears, and the space group changes into *Immm*. Bulk sodium nitrite melts at 554.1 K.

KDP and medium deuterated DKDP have tetragonal structure at the ambient temperature and undergoes a phase transition at about 123 K to ferroelectric phase with the space group (SG) *Fdd*2. The high-deuterated DKDP undergoes ferroelectric phase transition at 223 K. In the bulk KNO_3 crystals, ferroelectric phase is observed only when cooling at atmospheric pressure in the temperature range from 383 K to 398 K.

As porous matrices, we have used porous glasses with average pore diameters of 320 ± 20, 46 ± 5, 20 ± 3, 7 ± 1 and 3.0 ± 0.5 nm, ar-

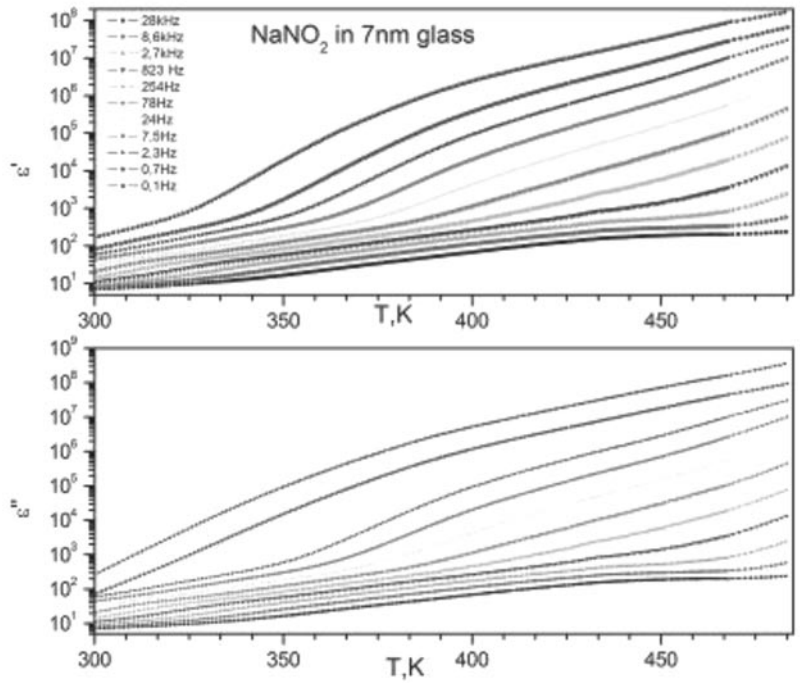

Fig. 9. Temperature dependences of real ε' and imaginary ε'' parts of dielectric response for $NaNO_2$ within 7 nm porous glasses at different frequencies

tificial opals and chrysotile asbestos with the average diameter of channels of 6 ± 1 nm. The samples with nanostructured $NaNO_2$ and KNO_3 were produced by immersion of empty vacuum dried porous glasses in the melted $NaNO_2$ (or KNO_3) for several hours. Due to high wetting ability these salts penetrate into the pores and fill about $22 - 25$ % of total sample volume. KDP, DKDP and Rochelle salt were prepared from water solutions of the salts. The filling in this case was about 10 % of the total sample volume.

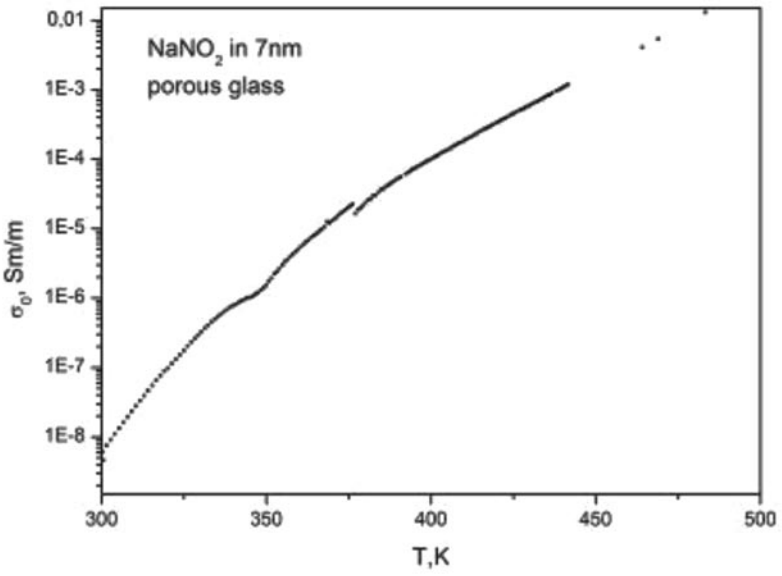

Fig. 10. Temperature dependences of NCM conductivity; $E_a \approx 0.96$ eV

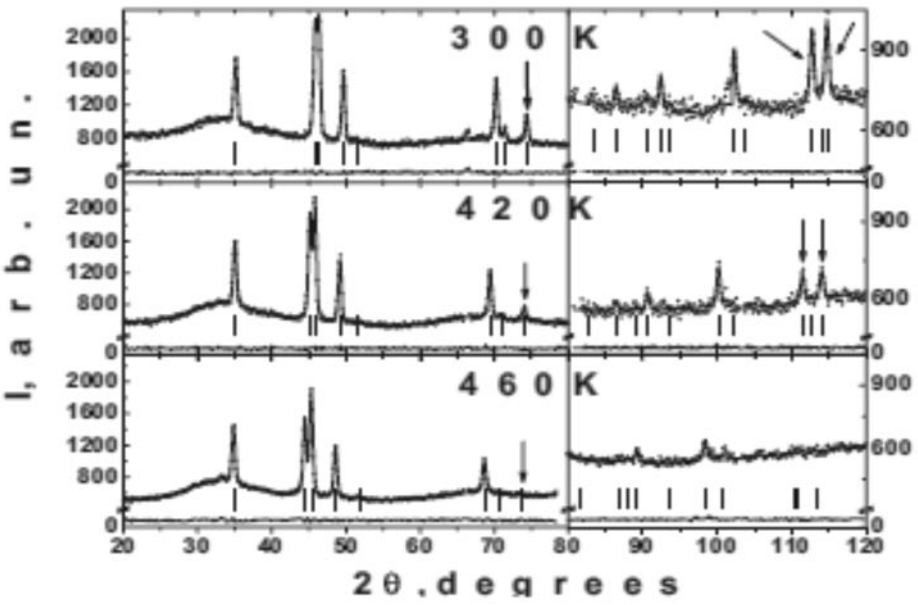

Fig. 11. Neutron diffraction patterns at 300 K, 420 K and 460 K. The arrows indicate the positions of (022), (132) and (123) Bragg peaks in the ferroelectric phase

B. Dielectric Data

In Fig. 9, the temperature dependences of real ε' and imaginary part ε'' of dielectric permittivity of NCM with $NaNO_2$ embedded into 7 nm porous glasses are presented. At low frequencies, the exponential growth of ε is observed. At 0.1 Hz the value of ε' achieves 10^8 at 490 K, but we have not observed the peak corresponding to the ferroelectric PT in the $\varepsilon(T)$ dependences. It links with great growth of conductivity in the vicinity of PT due to high mobility of sodium ions approaching (and above) T_C. The anomalies at T_C are observed on dependency $d\varepsilon'/dT$ only. From the analysis of dispersion curves, we have determined the parameters of relaxation phenomena and the value of DC (direct current) conductivity $\sigma(T)$ of NCM. This dependency is presented in Fig. 10 and follows Arrhenius law with activation energy ~ 1 eV.

C. Structure Evolution and Phase Transitions

The diffraction patterns at 300 K, 420 K (below T_C) and 460 K (above T_C) for sodium nitrite within 7 nm glasses are presented in Fig. 11. At all temperatures the structure of embedded sodium nitrite corresponds to the orthorhombic structure of the bulk $NaNO_2$, but in addition to normal diffraction peaks, a diffuse background due to scattering on porous silica glass is also observed. The widths of the observed diffraction peaks are larger than the instrumental resolution, but clearly smaller than the value expected for scattering on isolated 7 nm particles. The average size (≈ 45 nm) of clusters was determined from the structure refinement and was found to be practically temperature independent up to 460 K. Heating through T_C results in the decrease of intensity of most peaks at large scattering angles 2θ, i. e. at large $h\ k\ l$, and this effect is much stronger than in the bulk material. Above 523 K, we did not observe any diffraction peaks corresponding to the sodium nitrite structure, i. e. nanocomposite $NaNO_2$ melted entirely below the bulk T_{melt}. In the case of $NaNO_2$, there are two principal distinguishing groups of Bragg peaks: the intensity of diffraction peaks is proportional to

$$|F|^2 = F^2_{real} + \eta^2(T) \times F^2_{im},$$

where F_{real} and F_{im} are the real and imaginary parts of the structure factor F, and η is the order parameter for the ferroelectric phase.

For sodium nitrite, there are two families of reflections with different dependences on η: the first ones where $F_{im} \sim 0$ or $F^2_{im} << F^2_{real}$ (for example (110), (011), (101) and (200)) are

Table

Real and imaginary parts of the structure factor for sodium nitrite in the ferroelectric phase for different reflections

h	k	l	F^2_{real}	F^2_{im}
0	1	1	2.83	0.02
1	1	0	6.74	0.07
1	0	1	8.17	0
2	0	0	8.18	0
0	2	0	10.82	0.009
1	1	2	0.006	0.687
0	2	2	0.254	3.864
0	1	3	0.01	1.065
1	3	0	0.36	0.266
2	2	0	3.81	0.054
1	3	2	0.054	2.762
1	2	3	0.3	2.718
0	4	2	0.028	5.128

independent from the order parameter, and the second ones (the part of them marked by arrows in Fig. 11) where $F^2_{im} >> F^2_{real}$ ((022), (123), (132)). The values of F^2_{im} and F^2_{real} for different reflections in the ferroelectric phase are presented in the Table. It is easy to see that the intensities of these peaks are practically proportional to η^2. The curves $\eta(T)$ for NCM (Fig. 12) can be well fitted by the power law $(1 - T/T_C)^\beta$ with $T_C = 418.5 \pm 3.5$ and 423.6 ± 2.1 K for the 3 and 7 nm porous glasses correspondingly. The critical exponent β is equal to 0.33 ± 0.04 for both NCMs. This value of β is in a good agreement with the value (0.362 ± 0.004) obtained for the 3D Ising model [66] by computer simulation of finite-size scaling for a second order PT. The $\eta(T)$ curve for NCM for the 20 nm porous glass differs principally from those for nanocomposites with 3 and 7 nm pores and looks similar to the dependence obtained for the bulk [65]. The crossover of PT for small nanoparticles from the first order to the second order was confirmed by measuring heat capacity [67]. In Fig. 13, the temperature dependences of the unit cell volume for all types of NCM and for the bulk are presented. These curves for NCM are visibly different from that for the bulk. The appearance of the fast increase of the volume for

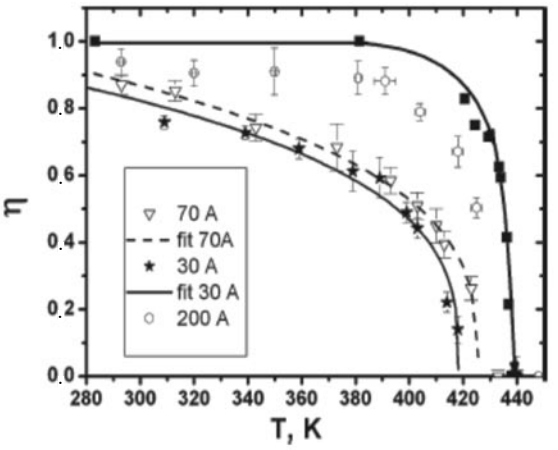

Fig. 12. Temperature dependences of the order parameter for the bulk (black squares) [65] and $NaNO_2$ embedded into porous glasses with average pore diameters 30 Å (stars), 70 Å (open triangles) and 200 Å (open circles)

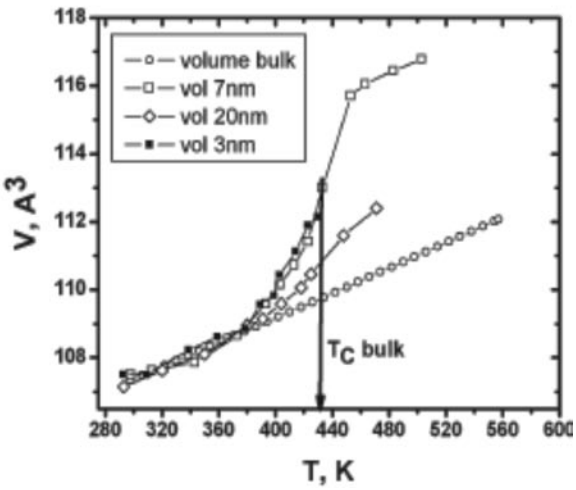

Fig. 13. Temperature dependences of the unit cell volume for 3 nm (black squares), 7 nm (open squares) and 20 nm (open rhombuses) porous glasses and the massive sodium nitrite

all NCMs is observed at ~380 K, i. e. below T_C, and at high temperature these values exceed the unit cell volume of bulk sodium nitrite in the vicinity of the melting point. Such a behavior can be considered as an evidence of lattice «softening» in NCM with 3 and 20 nm pores as it was proved earlier for sodium nitrite within 7 nm glasses. This essential increase of unit cell volume by ~8 % (and decrease of density) must lead to visible change of contrast at SANS. Indeed, it is easy to see in Fig. 14 that upon heat-

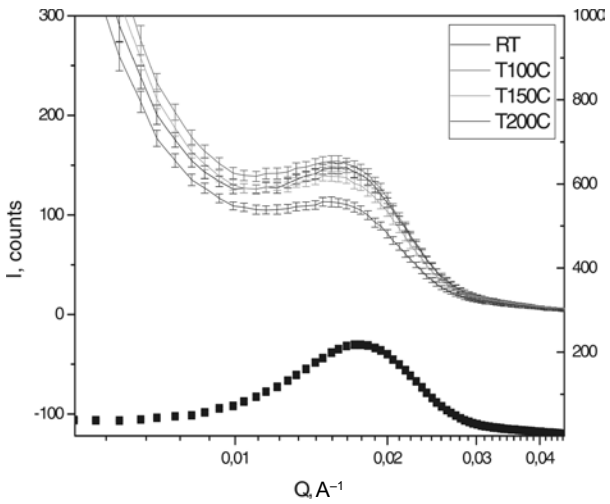

Fig. 14. Temperature dependences of intensity of SANS for $NaNO_2$ within 7 nm porous (glasses). Black line corresponds to scattering on empty porous glasses

ing through T_C (~164 °C), the contrast changes half as much at $Q \approx 0.018$ Å^{-1}.

D. Thermal Vibrations and Pre-Melted State

Analysis of neutron diffraction patterns permits us to obtain information concerning thermal motions of constituent ions of sodium nitrite within porous matrices.

The results at 420 K (below T_C) and 460 K (above T_C) are presented as ellipsoids of 50 % probability in Fig. 15 and as ellipsoids of 5 % probability in Fig. 16 (inasmuch as oxygen thermal displacements are very large for a porous sample). For the bulk material, these ellipsoids are close to a sphere at all temperatures, and the amplitudes of thermal motion do not change practically on heating throughout T_C. For confined sodium nitrit below T_C, these ellipsoids are clearly anisotro pic and slightly larger than for the bulk, bu upon heating through T_C, the picture change drastically. In the paraelectric phase (abov T_C), the vibrations of Na and N form practi cally flat disks perpendicular to the **b** direc tion for Na and the **a** direction for N as result of mixed rotation around the *a* and axes, while oxygen ions form very stretched ellipsoids predominantly along the *a* and *c* directions, as should be expected at increasing rotation around the *b* axis. The values of oxygen thermal displacements along the *c* and *a* directions at 460 K (above T_C) are equal to 1.21 and 0.93 E, respectively (i. e., more than 25 % of O—O (3.34 E) distance for neighboring NO_2 groups). These values essentially exceed the Lindemann criterion for melting. This experimental fact (and the sharp growth of unit cell volume upon heating through T_C) permits to conclude that above T_C and up to melting (~525 K), a specific volume pre-melted state with high mobility of constituent ions is formed in confined sodium nitrite at the temperature more than 100 K below the bulk T_{melt}. It is necessary to underline that this pre-melted state is not connected with very spreading surface (we have observed the diffraction peaks essentially above T_C), but it has a volume character and probably originates from some size effect of yet unclear nature. Measurements of NMR on ^{23}Na isotope confirm the growth (by ~20 times) of sodium mobility in this NCM upon heating [68].

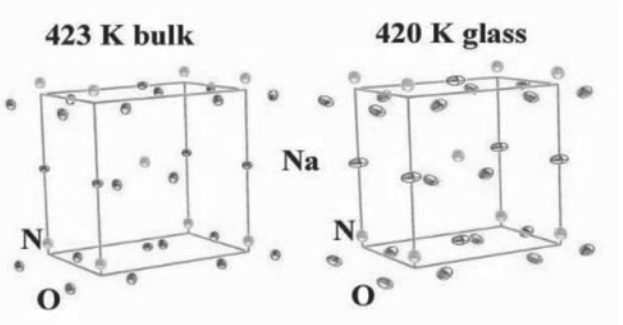

Fig. 15. Ellipsoids of thermal motions for the bulk (left) and confined within 7 nm porous glasses (right) $NaNO_2$ below T_C

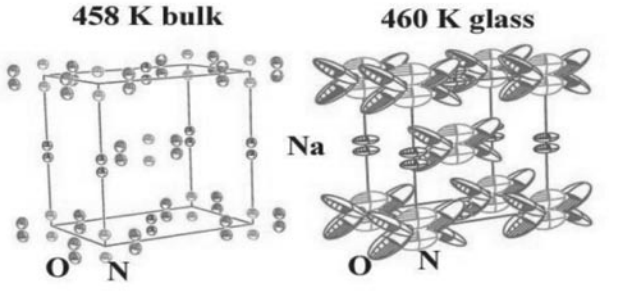

Fig. 16. Ellipsoids of thermal motions for the bulk (left) and confined within 7 nm porous glasses (right) $NaNO_2$ above T_C

E. Size Effect and Metastable Phases

The neutron diffraction patterns for high-deuterated DKDP show strong broadening of Bragg reflections due to a size-effect leading to large peak overlapping. Surprisingly, the measured patterns at all the temperatures appear to be inconsistent with the profiles simulated in the frame of the orthorhombic $Fdd2$ and tetragonal $I\bar{4}2d$ space groups (SG). From the comparison of the obtained diffraction patterns with the simulated ones, calculated for different crystal structures reported for DKDP (KDP) (see Table), it follows that the observed patterns can be best fitted by the monoclinic crystal structure with SG $P2_1$ and the unit-cell parameters close to the ones reported in [69] for high-deuterated DKDP. Unfortunately, the hydrogen positions for this monoclinic structure are unknown. Moreover, due to low symmetry and strong peak overlapping, it is impossible to refine these positions from our data. Therefore, we have refined the averaged diameter (size) of the embedded nanoparticles and the unit-cell parameters only in the so-called «matching mode» by the FULLPROF program. The temperature dependences of these parameters are shown in Fig. 17 and there are no anomalies in the temperature

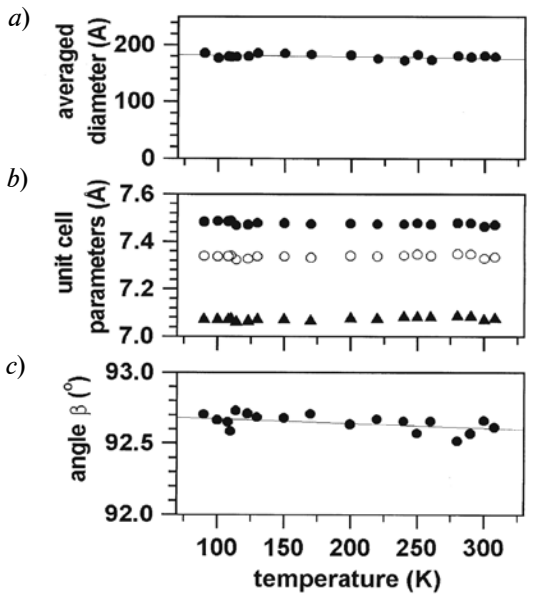

Fig. 17. Temperature dependences of refined averaged diameter of nanoparticles (*a*); unit cell parameters for monoclinic cells (*b*): *a* (solid circles), *b*/2 (open circles) and *c* (triangles); monoclinic angle β (*c*) for high-deuterated DKDP embedded into 7 nm porous glasses

interval of 90 – 308 K, i. e. the ferroelectric phase transition is absent in this temperature span for confined DKDP. It is shown that the

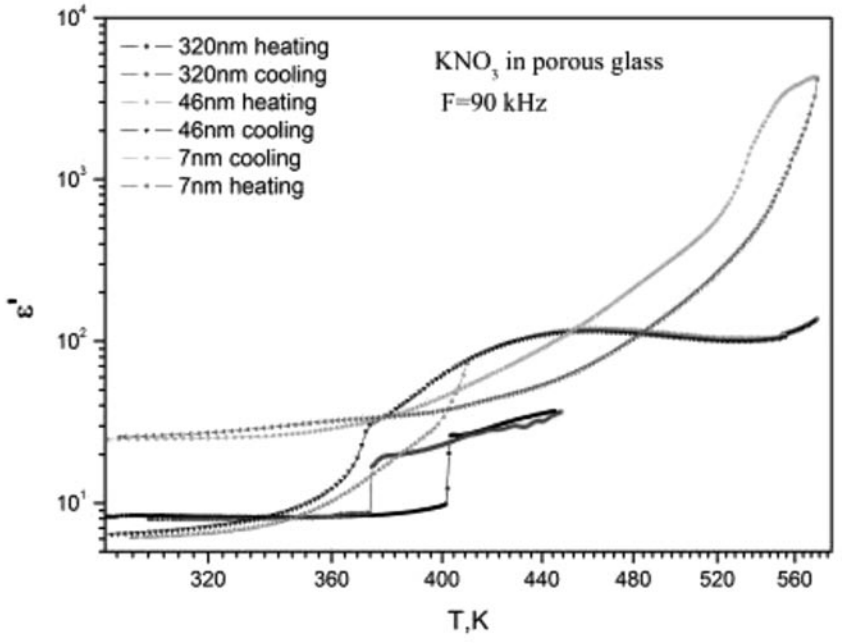

Fig. 18. Temperature dependences of the real part of dielectric permittivity for KNO_3 within various porous glasses on cooling and heating

monoclinic modification of the high-deuterated $K(D_{1-x}H_x)_2PO_4$ can exist at room temperature [70, 71] and crystallize from the high-deuterated (≈ 98%) aqueous solution only [70], but at ambient conditions this modification transforms into the tetragonal form in a few days [71]. Our samples with DKDP were crystallized from the aqueous solution too and were prepared some months before the beginning of the experiment and stored at ambient conditions. Therefore, the stability of the observed monoclinic phase is surprising. It is possible that such stability is associated with the size-effect and/or with peculiarities of the interaction of DKDP with porous matrix [72 – 74].

Some years ago, it was shown that thin films of KNO_3 exhibit ferroelectric properties at room temperature [75]. One of the simple ways to produce nano-sized ferroelectrics is introducing them into the porous glass matrices. As it is shown in the paper [64] for KNO_3 embedded into porous glasses, decreasing the pore diameter from 320 nm down to 46 nm leads to broadening the temperature range in which the metastable ferroelectric phase exists. In Fig. 18 the temperature dependencies of ε' on heating and cooling for KNO_3 embedded into 320, 46 and 7 nm porous glasses are presented. It is easy to see that the increase of nanoparticle sizes leads to smearing PT and to increasing thermal hysteresis. For NCM with 7 nm pores, a sharp growth of ε' due to potassium nitrate melting within pores is observed and T_{melt} in this case is essentially smaller than it is in the bulk (600 K).

IV. Summary

We have studied the physical properties and crystal structure of various ferroelectric and magnetic NCMs on the basis of porous matrices with different average pore diameters, and we can define some common features for these materials.

1. Embedding from wetting melt and chemical embedding produce nonspherical clusters with the average diameter which is larger than the pore diameter.

2. For some NCMs, there is a critical size of nanoparticles when the crossover of PT type is observed.

3. Examined ferroelectric NCMs with small particles demonstrate the giant dielectric permittivity in the paraelectric phase.

4. A new volume pre-melted state with extremely large thermal motions of constituent ions has been recovered for sodium nitrite.

5. The confinement can stabilize the phases that are usually metastable.

REFERENCES

1. **Zhong W.L., Wang Y.G., Zhang P.L.** Phase transitions in finite-size ferroelectrics. *Ferroelectr. Rev.*, 1998, 1, pp. 131–193.

2. **Neubeck W., Ranno L., Hunt M.B., Vettier C., Givord D.** Epitaxial MnO thin films grown by pulsed laser deposition. *Applied Surface Science*, 1999, 138, pp. 195–198.

3. **Li S., Eastman J.A., Li Z., Foster C.M., Newnham R.E., Cross L.E.** Size effects in nanostructured ferroelectrics. *Physics Letters A*, 1996, 212(6), pp. 341–346.

4. **Golosovsky I.V., Mirebeau I., André G., Kurdyukov D.A., Kumzerov Y.A., Vakhrushev S.B.** Magnetic ordering and phase transition in MnO embedded in a porous glass. *Physical Review Letters*, 2001, 86(25), 5783.

5. **Sheng P., Cohen R.W., Schrieffer J.R.** Melting transition of small molecular clusters. *Journal of Physics C: Solid State Physics*, 1981, 14(20), L565.

6. **Kumzerov Y.A., Nabereznov A.A., Vakhrushev S.B., Savenko B.N.** Freezing and melting of mercury in porous glass. *Physical Review B*, 1995, 52, pp. 4772–4774.

7. **Pan'kova S.V., Poborchii V.V., Solov'ev V.G.** The giant dielectric constant of opal containing sodium nitrate nanoparticles. *Journal of Physics: Condensed Matter*, 1996, 8(12), L203.

8. **Colla E.V., Fokin A.V., Kumzerov Y.A.** Ferroelectrics properties of nanosize KDP particles. *Solid State Communications*, 1997, 103(2), pp. 127–130.

9. **Colla E.V., Koroleva E.Y., Kumzerov Y.A., Savenko B.N., Vakhrushev S.B.** Ferroelectric phase transitions in materials embedded in porous media. *Ferroelectrics Letters Section*, 1996, 20(5–6), pp. 143–147.

10. **Beskrovny A., Golosovsky I., Fokin A., Kumzerov Y., Kurbakov A., Naberezhnov A., Vakhrushev S.** Structure evolution and formation of a pre-melted state in $NaNO_2$ confined within porous glass. *Applied Physics A*, 2002, 74(1), s1001–s1003.

11. **Fokin A.V., Kumzerov Y.A., Okuneva N.M., Naberezhnov A.A., Vakhrushev S.B., Golosovsky I.V., Kurbakov A.I.** Temperature evolution of sodium nitrite structure in a restricted geometry. *Physical Review Letters*, 2002, 89(17), 175503.

12. **Charnaya E.V., Loeser T., Michel D., Tien C., Yaskov D., Kumzerov Y.A.** Spin-lattice relaxation enhancement in liquid gallium confined within nanoporous matrices. *Physical Review Letters*, 2002, 88(9), 097602.

13. **Drake J.M., Grest G.S., Klafter J., Kopelman R.** Dynamics in Small Confining Systems. Pittsburgh, PA, Materials Research Society, 1999.

14. **Graf M.J., Huber T.E., Huber C.A.** Superconducting properties of indium in the restricted geometry of porous Vycor glass. *Physical Review B*, Eds., 1992. 45(6), 3133.

15. **Charnaya E.V., Tien C., Lin K.J., Wur C.S., Kumzerov Y.A.** Superconductivity of gallium in various confined geometries. *Physical Review B*, 1998, 58(1), 467.

16. **Panova G.K., Naberezhnov A.A., Fokin A.V.** Surface and volume superconductivity of Pb embedded in nanopores. *Physics of the Solid State*, 2008, 50(7), pp. 1370–1373.

17. **Chan M.H.W., Blum K.I., Murphy S.Q., Wong G.K.S., Reppy J.D.** Disorder and the superfluid transition in liquid^{4} He. *Physical Review Letters*, 1988, 61(17), 1950.

18. **Larson M., Mulders N., Ahlers G.** Thermal expansion coefficient near the superfluid transition of^{4} He in an aerogel. *Physical Review Letters*, 1992, 68(26), 3896.

19. **Mu R., Malhotra V.M.** Effects of surface and physical confinement on the phase transitions of cyclohexane in porous silica. *Physical Review B*, 1991, 44(9), 4296.

20. **Duffy J.A., Wilkinson N.J., Fretwell H.M., Alam M.A., Evans R.** Phase transitions of CO_2 confined in nanometer pores as revealed by positronium annihilation. *Journal of Physics: Condensed Matter*, 1995, 7(50), L713.

21. **Jackson C.L., & McKenna G.B.** The melting behavior of organic materials confined in porous solids. *The Journal of Chemical Physics*, 1990, 93, 9002.

22. **Beamish J.R., Hikata A., Tell L., Elbaum C.** Solidification and superfluidity of/sup 4/He in porous Vycor glass. *Physical Review Letters*, 1983, 50(6).

23. **Borisov B.F., Charnaya E.V., Plotnikov P.G., Hoffmann W.D., Michel D., Kumzerov Y.A. [et al.].** Solidification and melting of mercury in a porous glass as studied by NMR and acoustic techniques. *Physical Review B*, 1998, 58(9), 5329.

24. **Bellissent-Funel M.C., Lal J., Bosio L.** Structural study of water confined in porous glass by neutron scattering. *The Journal of Chemical Physics*, 1993, 98, 4246.

25. **Kanata T., Yoshikawa T., Kubota K.** Grain-size effects on dielectric phase transition of $BaTiO_3$ ceramics. *Solid State Communications*, 1987, 62(11), pp. 765–767.

26. **Ishikawa K., Yoshikawa K., Okada N.** Size effect on the ferroelectric phase transition in PbTiO_{3} ultrafine particles. *Physical Review B*, 1988, 37(10), 5852.

27. **Colla E.V., Fokin A.V., Koroleva E.Y., Kumzerov Y.A., Vakhrushev S.B., Savenko B.N.** Ferroelectric phase transitions in materials embedded in porous media. *Nanostructured Materials*, 1999, 12(5), pp. 963–966.

28. **Anliker K., Brugger H.R., and Кдnzig W.** *Helv. Phys.Acta*, 1954, Vol. 27, p. 99 .

29. **Saegusa K., Rhine W.E., Bowen H.K.** Effect of composition and size of crystallite on crystal phase in lead barium titanate. *Journal of the American Ceramic Society*, 1993, 76(6), pp. 1505–1512.

30. **Uchino K., Sadanaga E., Hirose T.** Dependence of the crystal structure on particle size in barium titanate. *Journal of the American Ceramic Society*, 1989, 72(8), pp. 1555–1558.

31. **Marquardt P., Gleiter H.** Ferroelectric phase transition in microcrystals. *Physical Review Letters*, 1982, 48, pp. 1423–1424.

32. **Zhong W.L., Wang Y.G., Zhang P.L.** Size effects on phase transitions in ferroelectric films. *Physics letters A*, 1994, 189(1), pp. 121–126.

33. **Buchheit W., Kreibig U., Мыller D., Voigt A.** NMR of ^{23}Na in small particles of ferroelectric $NaNO_2$. *Zeitschrift für Physik B. Condensed Matter*, 1978, 2(1), pp. 83–91.

34. **Vakhrushev S.B., Kumzerov Y.A., Fokin A., Naberezhnov A.A., Zalar B., Lebar A., Blinc R.** ^{23} Na spin-lattice relaxation of sodium nitrite in confined geometry. *Physical Review B*, 2004, 70(13), 132102.

35. **Steytler D.C., Dore J.C., Wright C.J.** Neutron diffraction study of cubic ice nucleation in a porous silica network. *The Journal of Physical Chemistry*, 1983, 87(14), pp. 2458–2459.

36. **Wiltzius P., Bates F.S., Dierker S.B., Wignall G.D.** Structure of porous Vycor glass. *Physical Review A*, 1987, 36(6), 2991.

37. **Koroleva E.Y., Nuzhnyy D., Pokorny J., Kamba S., Kumzerov Y.A., Vakhrushev S.B., Petzelt J.** The negative phonon confinement effect in nanoscopic sodium nitrite. *Nanotechnology*, 2009, 20(39), 395706.

38. **Saegusa K., Rhine W.E., Bowen H.K.** Effect of composition and size of crystallite on crystal phase in lead barium titanate. *Journal of the American*

Ceramic Society, 1993, 76(6), pp. 1505–1512.

39. **Colla E.V., Fokin A.V., Koroleva E.Y., Kumzerov Y.A., Vakhrushev S.B., Savenko B.N.** Ferroelectric phase transitions in materials embedded in porous media. *Nanostructured Materials*, 1999, 12(5), pp. 963–966.

40. **Steytler D.C., Dore J.C., Wright C.J.** Neutron diffraction study of cubic ice nucleation in a porous silica network. *The Journal of Physical Chemistry*, 1983, 87(14), pp. 2458–2459.

41. **Dore J.C., Dunn M., Chieux P.** Neutron diffraction studies of ice nucleation in porous silica. *Le Journal de Physique Colloques*, 1987, 48(C1), pp. C1–457.

42. **Benham M.J., Cook J.C., Li J.C., Ross D.K., Hall P.L., & Sarkissian B.** Small-angle neutron scattering study of adsorbed water in porous Vycor glass: Supercooling phase transition and interfacial structure. *Physical Review B*, 1989, 39(1), 633.

43. **Wiltzius P., Bates F.S., Dierker S.B., Wignall G.D.** Structure of porous Vycor glass. *Physical Review A*, 1987, 36(6), 2991.

44. **Naberezhnov A., Fokin A., Kumzerov Y., Sotnikov A., Vakhrushev S., Dorner B.** Structure and properties of confined sodium nitrite. *The European Physical Journal E*, 2003, 12(1), pp. 21–24.

45. **Golosovsky I.V., Delaplane R.G., Naberezhnov A.A., Kumzerov Y.A.** Thermal motion in lead confined within a porous glass. *Physical Review B*, 2004, 69(13), 132301.

46. **Golosovsky I.V., Mirebeau I., Elkaim E., Kurdyukov D.A., Kumzerov Y.A.** Structure of MnO nanoparticles embedded into channel-type matrices. *The European Physical Journal B. Condensed Matter and Complex Systems*, 2005, 47(1), pp. 55–62.

47. **Golosovsky I.V., Salazar-Alvarez G., Lypez-Ortega A., González M.A., Sort J., Estrader M., Nogués J.** Magnetic proximity effect features in antiferromagnetic/ferrimagnetic core-shell nanoparticles. *Physical Review Letters*, 2009, 102(24), 247201.

48. **Marquardt P., Gleiter H.** Ferroelectric phase transition in microcrystals. *Physical Review Letters*, 1982, 48, pp. 1423–1424.

49. **Shull C.G., Strauser W.A., Wollan E.O.** Neutron diffraction by paramagnetic and antiferromagnetic substances. *Physical Review*, 1951, 83(2), 333.

50. **Roth W.L.** Magnetic structures of MnO, FeO, CoO, and NiO. *Physical Review*, 1958, 110(6), 1333.

51. **Lines M.E., Jones E.D.** Antiferromagnetism in the face-centered cubic lattice. II. Magnetic properties of MnO. *Physical Review*, 1965, 139(4A), A1313.

52. **Rodbell D.S., Owen J.** Sublattice magnetization and lattice distortions in MnO and NiO. *Journal of Applied Physics*, 1964, 35, 1002.

53. **Golosovsky I.V., Arčon D., Jagličič Z., Cevc P., Sakhnenko V.P., Kurdyukov D.A., Kumzerov Y.A.** ESR studies of MnO embedded into silica nanoporous matrices with different topology. *Physical Review B*. 2005, 2(14), 144410.

54. **Dronskowski R.** The little maghemite story: A classic functional material. *Advanced Functional Materials*, 2001, 11(1), pp. 27–29.

55. **Golosovsky I.V., Tovar M., Hoffman U., Mirebeau I., Fauth F., Kurdyukov D.A., Kumzerov Y.A.** Diffraction studies of the crystalline and magnetic structures of γ-Fe_2O_3 iron oxide nanostructured in porous glass. *Journal of Experimental and Theoretical Physics Letters*, 2006, 83(7), pp. 298–301.

56. **Golosovsky I.V., Mirebeau I., Fauth F., Kurdyukov D.A., Kumzerov Y.A.** Magnetic structure of hematite nanostructured in a porous glass. *Solid State Communications*, 2007, 141(4), pp. 178–182.

57. **Cabrera G.G.** First order phase transitions in a solid with finite size. *International Journal of Modern Physics B*, 1990, 4(10), pp. 1671–1692.

58. **Binder K., Landau D.P.** Finite-size scaling at first-order phase transitions. *Physical Review B*, 1984, 30(3), 1477.

59. **Barber M.N.** Phase transitions and critical phenomena, Vol. 8, ed. C. Domb and L. Lebowitz. New York: Academic, 1983. 145 p.

60. **Golosovsky I.V., Mirebeau I., André G., Tovar M., Tobbens D.M., Kurdyukov D.A., Kumzerov Y.A.** Magnetic phase transition in a nanostructured antiferromagnet CoO embedded in porous glass. *Physics of the Solid State*, 2006, 48(11), pp. 2130–2133.

61. **Salazar-Alvarez G., Sort J., Surinach S., Baró M.D., Nogués J.** Synthesis and size-dependent exchange bias in inverted core-shell MnO/Mn_3O_4 nanoparticles. *Journal of the American Chemical Society*, 2007, 129(29), pp. 9102–9108.

61a. **Berkowitz A.E., Rodriguez G.F., Hong J.I., An K., Hyeon T., Agarwal N. [et al.].** Antiferromagnetic MnO nanoparticles with ferrimagnetic Mn_3O_4 shells: Doubly inverted core-shell system. *Physical Review B*, 2008, 77(2), 024403.

62. **Poprawski R., Rysiakiewicz-Pasek E., Sieradzki A., Ciżman A., Polańska J.** Ferroelectric phase transitions in KNO_3 embedded into porous glasses. *Journal of Non-Crystalline Solids*, 2007, 353(47), pp. 4457–4461.

62a. **da Costa Lamas A., Chang S.L., Caticha-Ellis S.** On the use of powder diffractometry in the study of phase transitions case of $NaNO_2$. *Physica Status Solidi (A)*, 1981, 68(1), pp. 173–178.

63. **Landau D.P.** Computer simulation studies of magnetic phase transitions. *Journal of Magnetism and Magnetic Materials*, 1999, 200(1), pp. 231–247.

64. **Kutnjak Z., Vodopivec B., Blinc R., Fokin A.V., Kumzerov Y.A., Vakhrushev S.B.** Calorimetric and dielectric studies of ferroelectric sodium nitrite confined in a nanoscale porous glass matrix. *The Journal of Chemical Physics*, 2005, 123, 084708.

65. **Vakhrushev S.B., Kumzerov Y.A., Fokin A., Naberezhnov A.A., Zalar B., Lebar A., Blinc R.** ^{23}Na spin-lattice relaxation of sodium nitrite in confined geometry. *Physical Review B*, 2004, 70(13), 132102.

66. **Nelmes R.J.** The crystal structure of monoclinic KD_2PO_4. *Physica Status Solidi (B)*, 1972, 52(2), pp. K89–K93.

67. **Itoh K., Matsubayashi T., Nakamura E., Motegi H.** *X*-ray study of high-temperature phase transitions in KH_2PO_4. *Journal of the Physical Society of Japan*, 1975, 39, 843.

68. **Mathew M., Wong-Ng** W. Crystal structure of a new monoclinic form of potassium dihydrogen phosphate containing orthophosphacidium ion, $[H_4PO_4]^{+1}$. *Journal of Solid State Chemistry*, 1995, 114(1), pp. 219–223.

69. **Burkovsky R.G., Filimonov A.V., Rudskoy A.I., Hirota K., Matsuura M., Vakhrushev S.B.** Diffuse scattering anisotropy and inhomogeneous lattice deformations in the lead magnoniobate relaxor PMN above the Burns temperature. *Physical Review B*, 2012, 85(9), 094108.

70. **Burkovsky R.G., Bronwald Y.A., Filimonov A.V., Rudskoy A.I., Chernyshov D., Bosak A. [et al.].** Structural heterogeneity and diffuse scattering in morphotropic lead zirconate-titanate single crystals. *Physical Review Letters*, 2012, 109(9), 097603.

71. **Tagantsev A.K., Vaideeswaran K., Vakhrushev S.B., Filimonov A.V., Burkovsky R.G., Shaganov A. [et al.].** The origin of antiferroelectricity in $PbZrO_3$. *Nature communications*, 2013, 4.

72. **Scott J.F., Duiker H.M., Beale P.D., Pouligny B., Dimmler K., Parris M. [et al.].** Properties of ceramic KNO_3 thin-film memories. *Physica B+C*, 1988, 150(1), pp. 160–167.

СПИСОК ЛИТЕРАТУРЫ

1. **Zhong W.L., Wang Y.G., Zhang P.L.** Phase transitions in finite-size ferroelectrics. *Ferroelectr. Rev.*, 1998, 1, pp. 131–193.

2. **Neubeck W., Ranno L., Hunt M.B., Vettier C., Givord D.** Epitaxial MnO thin films grown by pulsed laser deposition. *Applied Surface Science*, 1999, 138, pp. 195–198.

3. **Li S., Eastman J.A., Li Z., Foster C.M., Newnham R.E., Cross L.E.** Size effects in nanostructured ferroelectrics. *Physics Letters A*, 1996, 212(6), pp. 341–346.

4. **Golosovsky I.V., Mirebeau I., Andrй G., Kurdyukov D.A., Kumzerov Y.A., Vakhrushev S.B.** Magnetic ordering and phase transition in MnO embedded in a porous glass. *Physical Review Letters*, 2001, 86(25), 5783.

5. **Sheng P., Cohen R.W., Schrieffer J.R.** Melting transition of small molecular clusters. *Journal of Physics C: Solid State Physics*, 1981, 14(20), L565.

6. **Kumzerov Y.A., Nabereznov A.A., Vakhrushev S.B., Savenko B.N.** Freezing and melting of mercury in porous glass. *Physical Review B*, 1995, 52, pp. 4772–4774.

7. **Pan'kova S.V., Poborchii V.V., Solov'ev V.G.** The giant dielectric constant of opal containing sodium nitrate nanoparticles. *Journal of Physics: Condensed Matter*, 1996, 8(12), L203.

8. **Colla E.V., Fokin A.V., Kumzerov Y.A.** Ferroelectrics properties of nanosize KDP particles. *Solid State Communications*, 1997, 103(2), pp. 127–130.

9. **Colla E.V., Koroleva E.Y., Kumzerov Y.A., Savenko B.N., Vakhrushev S.B.** Ferroelectric phase transitions in materials embedded in porous media. *Ferroelectrics Letters Section*, 1996, 20(5–6), pp. 143–147.

10. **Beskrovny A., Golosovsky I., Fokin A., Kumzerov Y., Kurbakov A., Naberezhnov A., Vakhrushev S.** Structure evolution and formation of a pre–melted state in $NaNO_2$ confined within porous glass. *Applied Physics A*, 2002, 74(1), s1001–s1003.

11. **Fokin A.V., Kumzerov Y.A., Okuneva N.M., Naberezhnov A.A., Vakhrushev S.B., Golosovsky I.V., Kurbakov A.I.** Temperature evolution of sodium nitrite structure in a restricted geometry. *Physical Review Letters*, 2002, 89(17), 175503.

12. **Charnaya E.V., Loeser T., Michel D., Tien C., Yaskov D., Kumzerov Y.A.** Spin-lattice relaxation enhancement in liquid gallium confined within nanoporous matrices. *Physical Review Letters*, 2002, 88(9), 097602.

13. **Drake J.M., Grest G.S., Klafter J., Kopelman R.** Dynamics in Small Confining Systems. Pittsburgh, PA, Materials Research Society, 1999.

14. **Graf M.J., Huber T.E., Huber C.A.** Superconducting properties of indium in the restricted geometry of porous Vycor glass. *Physical Review B*, Eds., 1992. 45(6), 3133.

15. **Charnaya E.V., Tien C., Lin K.J., Wur C.S., Kumzerov Y.A.** Superconductivity of gallium in various confined geometries. *Physical Review B*, 1998, 58(1), 467.

16. **Panova G.K., Naberezhnov A.A., Fokin**

A.V. Surface and volume superconductivity of Pb embedded in nanopores. *Physics of the Solid State*, 2008, 50(7), pp. 1370–1373.

17. **Chan M.H.W., Blum K.I., Murphy S.Q., Wong G.K.S., Reppy J.D.** Disorder and the superfluid transition in liquid^{4} He. *Physical Review Letters*, 1988, 61(17), 1950.

18. **Larson M., Mulders N., Ahlers G.** Thermal expansion coefficient near the superfluid transition of^{4} He in an aerogel. *Physical Review Letters*, 1992, 68(26), 3896.

19. **Mu R., Malhotra V.M.** Effects of surface and physical confinement on the phase transitions of cyclohexane in porous silica. *Physical Review B*, 1991, 44(9), 4296.

20. **Duffy J.A., Wilkinson N.J., Fretwell H.M., Alam M.A., Evans R.** Phase transitions of CO_2 confined in nanometer pores as revealed by positronium annihilation. *Journal of Physics: Condensed Matter*, 1995, 7(50), L713.

21. **Jackson C.L., & McKenna G.B.** The melting behavior of organic materials confined in porous solids. *The Journal of Chemical Physics*, 1990, 93, 9002.

22. **Beamish J.R., Hikata A., Tell L., Elbaum C.** Solidification and superfluidity of/sup 4/He in porous Vycor glass. *Physical Review Letters*, 1983, 50(6).

23. **Borisov B.F., Charnaya E.V., Plotnikov P.G., Hoffmann W.D., Michel D., Kumzerov Y.A. [et al.].** Solidification and melting of mercury in a porous glass as studied by NMR and acoustic techniques. *Physical Review B*, 1998, 58(9), 5329.

24. **Bellissent-Funel M.C., Lal J., Bosio L.** Structural study of water confined in porous glass by neutron scattering. *The Journal of Chemical Physics*, 1993, 98, 4246.

25. **Kanata T., Yoshikawa T., Kubota K.** Grain-size effects on dielectric phase transition of $BaTiO_3$ ceramics. *Solid State Communications*, 1987, 62(11), pp. 765–767.

26. **Ishikawa K., Yoshikawa K., Okada N.** Size effect on the ferroelectric phase transition in PbTiO_ {3} ultrafine particles. *Physical Review B*, 1988, 37(10), 5852.

27. **Colla E.V., Fokin A.V., Koroleva E.Y., Kumzerov Y.A., Vakhrushev S.B., Savenko B.N.** Ferroelectric phase transitions in materials embedded in porous media. *Nanostructured Materials*, 1999, 12(5), pp. 963–966.

28. **Anliker K., Brugger H.R., and Кдnzig W.** *Helv. Phys.Acta*, 1954, Vol. 27, p. 99 .

29. **Saegusa K., Rhine W.E., Bowen H.K.** Effect of composition and size of crystallite on crystal phase in lead barium titanate. *Journal of the American Ceramic Society*, 1993, 76(6), pp. 1505–1512.

30. **Uchino K., Sadanaga E., Hirose T.** Dependence of the crystal structure on particle size in barium titanate. *Journal of the American Ceramic Society*, 1989, 72(8), pp. 1555–1558.

31. **Marquardt P., Gleiter H.** Ferroelectric phase transition in microcrystals. *Physical Review Letters*, 1982, 48, pp. 1423–1424.

32. **Zhong W.L., Wang Y.G., Zhang P.L.** Size effects on phase transitions in ferroelectric films. *Physics letters A*, 1994, 189(1), pp. 121–126.

33. **Buchheit W., Kreibig U., Mьller D., Voigt A.** NMR of ^{23}Na in small particles of ferroelectric $NaNO_2$. *Zeitschrift für Physik B. Condensed Matter*, 1978, 2(1), pp. 83–91.

34. **Vakhrushev S.B., Kumzerov Y.A., Fokin A., Naberezhnov A.A., Zalar B., Lebar A., Blinc R.** ^{23} Na spin-lattice relaxation of sodium nitrite in confined geometry. *Physical Review B*, 2004, 70(13), 132102.

35. **Steytler D.C., Dore J.C., Wright C.J.** Neutron diffraction study of cubic ice nucleation in a porous silica network. *The Journal of Physical Chemistry*, 1983, 87(14), pp. 2458–2459.

36. **Wiltzius P., Bates F.S., Dierker S.B., Wignall G.D.** Structure of porous Vycor glass. *Physical Review A*, 1987, 36(6), 2991.

37. **Koroleva E.Y., Nuzhnyy D., Pokorny J., Kamba S., Kumzerov Y.A., Vakhrushev S.B., Petzelt J.** The negative phonon confinement effect in nanoscopic sodium nitrite. *Nanotechnology*, 2009, 20(39), 395706.

38. **Saegusa K., Rhine W.E., Bowen H.K.** Effect of composition and size of crystallite on crystal phase in lead barium titanate. *Journal of the American Ceramic Society*, 1993, 76(6), pp. 1505–1512.

39. **Colla E.V., Fokin A.V., Koroleva E.Y., Kumzerov Y.A., Vakhrushev S.B., Savenko B.N.** Ferroelectric phase transitions in materials embedded in porous media. *Nanostructured Materials*, 1999, 12(5), pp. 963–966.

40. **Steytler D.C., Dore J.C., Wright C.J.** Neutron diffraction study of cubic ice nucleation in a porous silica network. *The Journal of Physical Chemistry*, 1983, 87(14), pp. 2458–2459.

41. **Dore J.C., Dunn M., Chieux P.** Neutron diffraction studies of ice nucleation in porous silica. *Le Journal de Physique Colloques*, 1987, 48(C1), pp. C1–457.

42. **Benham M.J., Cook J.C., Li J.C., Ross D.K., Hall P.L., & Sarkissian B.** Small-angle neutron scattering study of adsorbed water in porous Vycor glass: Supercooling phase transition and interfacial structure. *Physical Review B*, 1989, 39(1), 633.

43. **Wiltzius P., Bates F.S., Dierker S.B., Wignall G.D.** Structure of porous Vycor glass. *Physical Review A*, 1987, 36(6), 2991.

44. **Naberezhnov A., Fokin A., Kumzerov Y., Sotnikov A., Vakhrushev S., Dorner B.** Structure and properties of confined sodium nitrite. *The European Physical Journal E*, 2003, 12(1), pp. 21–24.

45. **Golosovsky I.V., Delaplane R.G., Naberezhnov A.A., Kumzerov Y.A.** Thermal motion in lead confined within a porous glass. *Physical Review B*, 2004, 69(13), 132301.

46. **Golosovsky I.V., Mirebeau I., Elkaim E., Kurdyukov D.A., Kumzerov Y.A.** Structure of MnO nanoparticles embedded into channel-type matrices. *The European Physical Journal B. Condensed Matter and Complex Systems*, 2005, 47(1), pp. 55–62.

47. **Golosovsky I.V., Salazar-Alvarez G., Lypez-Ortega A., González M.A., Sort J., Estrader M., Nogués J.** Magnetic proximity effect features in antiferromagnetic/ferrimagnetic core-shell nanoparticles. *Physical Review Letters*, 2009, 102(24), 247201.

48. **Marquardt P., Gleiter H.** Ferroelectric phase transition in microcrystals. *Physical Review Letters*, 1982, 48, pp. 1423–1424.

49. **Shull C.G., Strauser W.A., Wollan E.O.** Neutron diffraction by paramagnetic and antiferromagnetic substances. *Physical Review*, 1951, 83(2), 333.

50. **Roth W.L.** Magnetic structures of MnO, FeO, CoO, and NiO. *Physical Review*, 1958, 110(6), 1333.

51. **Lines M.E., Jones E.D.** Antiferromagnetism in the face-centered cubic lattice. II. Magnetic properties of MnO. *Physical Review*, 1965, 139(4A), A1313.

52. **Rodbell D.S., Owen** J. Sublattice magnetization and lattice distortions in MnO and NiO. *Journal of Applied Physics*, 1964, 35, 1002.

53. **Golosovsky I.V., Arčon D., Jagličič Z., Cevc P., Sakhnenko V.P., Kurdyukov D.A., Kumzerov Y.A.** ESR studies of MnO embedded into silica nanoporous matrices with different topology. *Physical Review B.* 2005, 2(14), 144410.

54. **Dronskowski R.** The little maghemite story: A classic functional material. *Advanced Functional Materials*, 2001, 11(1), pp. 27–29.

55. **Golosovsky I.V., Tovar M., Hoffman U., Mirebeau I., Fauth F., Kurdyukov D.A., Kumzerov Y.A.** Diffraction studies of the crystalline and magnetic structures of γ-Fe_2O_3 iron oxide nanostructured in porous glass. *Journal of Experimental and Theoretical Physics Letters*, 2006, 83(7), pp. 298–301.

56. **Golosovsky I.V., Mirebeau I., Fauth F., Kurdyukov D.A., Kumzerov Y.A.** Magnetic structure of hematite nanostructured in a porous glass. *Solid State Communications*, 2007, 141(4), pp. 178–182.

57. **Cabrera G.G.** First order phase transitions in a solid with finite size. *International Journal of Modern Physics B*, 1990, 4(10), pp. 1671–1692.

58. **Binder K., Landau D.P.** Finite-size scaling at first-order phase transitions. *Physical Review B*, 1984, 30(3), 1477.

59. **Barber M.N.** Phase transitions and critical phenomena, Vol. 8, ed. C. Domb and L. Lebowitz. New York: Academic, 1983. 145 p.

60. **Golosovsky I.V., Mirebeau I., André G., Tovar M., Tobbens D.M., Kurdyukov D.A., Kumzerov Y.A.** Magnetic phase transition in a nanostructured antiferromagnet CoO embedded in porous glass. *Physics of the Solid State*, 2006, 48(11), pp. 2130–2133.

61. **Salazar-Alvarez G., Sort J., Surinach S., Baró M.D., Nogués J.** Synthesis and size-dependent exchange bias in inverted core-shell MnO/Mn_3O_4 nanoparticles. *Journal of the American Chemical Society*, 2007, 129(29), pp. 9102–9108.

61a. **Berkowitz A.E., Rodriguez G.F., Hong J.I., An K., Hyeon T., Agarwal N. [et al.].** Antiferromagnetic MnO nanoparticles with ferrimagnetic Mn_3O_4 shells: Doubly inverted core-shell system. *Physical Review B*, 2008, 77(2), 024403.

62. **Poprawski R., Rysiakiewicz-Pasek E., Sieradzki A., Ciżman A., Polańska J.** Ferroelectric phase transitions in KNO_3 embedded into porous glasses. *Journal of Non-Crystalline Solids*, 2007, 353(47), pp. 4457–4461.

62a. **da Costa Lamas A., Chang S.L., Caticha-Ellis S.** On the use of powder diffractometry in the study of phase transitions case of $NaNO_2$. *Physica Status Solidi (A)*, 1981, 68(1), pp. 173–178.

63. **Landau D.P.** Computer simulation studies of magnetic phase transitions. *Journal of Magnetism and Magnetic Materials*, 1999, 200(1), pp. 231–247.

64. **Kutnjak Z., Vodopivec B., Blinc R., Fokin A.V., Kumzerov Y.A., Vakhrushev S.B.** Calorimetric and dielectric studies of ferroelectric sodium nitrite confined in a nanoscale porous glass matrix. *The Journal of Chemical Physics*, 2005, 123, 084708.

65. **Vakhrushev S.B., Kumzerov Y.A., Fokin A., Naberezhnov A.A., Zalar B., Lebar A., Blinc R.** ^{23}Na spin-lattice relaxation of sodium nitrite in confined geometry. *Physical Review B*, 2004, 70(13), 132102.

66. **Nelmes R.J.** The crystal structure of monoclinic KD_2PO_4. *Physica Status Solidi (B)*, 1972, 52(2), pp. K89–K93.

67. **Itoh K., Matsubayashi T., Nakamura E., Motegi H.** *X*-ray study of high-temperature phase transitions in KH_2PO_4. *Journal of the Physical Society of Japan*, 1975, 39, 843.

68. **Mathew M., Wong-Ng** W. Crystal structure of a new monoclinic form of potassium dihydrogen phosphate containing orthophosphacidium ion,

$[H_4PO_4]^{+1}$. *Journal of Solid State Chemistry*, 1995, 114(1), pp. 219–223.

69. **Burkovsky R.G., Filimonov A.V., Rudskoy A.I., Hirota K., Matsuura M., Vakhrushev S.B.** Diffuse scattering anisotropy and inhomogeneous lattice deformations in the lead magnoniobate relaxor PMN above the Burns temperature. *Physical Review B*, 2012, 85(9), 094108.

70. **Burkovsky R.G., Bronwald Y.A., Filimonov A.V., Rudskoy A.I., Chernyshov D., Bosak A. [et al.].** Structural heterogeneity and diffuse scattering in morphotropic lead zirconate-titanate single crystals. *Physical Review Letters*, 2012, 109(9), 097603.

71. **Tagantsev A.K., Vaideeswaran K., Vakhrushev S.B., Filimonov A.V., Burkovsky R.G., Shaganov A. [et al.].** The origin of antiferroelectricity in $PbZrO_3$. *Nature communications*, 2013, 4.

72. **Scott J.F., Duiker H.M., Beale P.D., Pouligny B., Dimmler K., Parris M. [et al.].** Properties of ceramic KNO_3 thin-film memories. *Physica B+C*, 1988, 150(1), pp. 160–167.

ФИЛИМОНОВ Алексей Владимирович – *доктор физико-математических наук, доцент кафедры физической электроники Санкт-Петербургского государственного политехнического университета.*
195251, Россия, Санкт-Петербург, Политехническая ул., 29
filimonov@rphf.spbstu.ru

РУДСКОЙ Андрей Иванович – *доктор технических наук, член-корреспондент РАН, заведующий кафедрой пластической обработки металлов Санкт-Петербургского государственного политехнического университета.*
195251, Россия, Санкт-Петербург, Политехническая ул., 29
rector@spbstu.ru

НАБЕРЕЖНОВ Александр Алексеевич – *кандидат физико-математических наук, старший научный сотрудник лаборатории нейтронных исследований Физико-технического института им. А.Ф. Иоффе РАН.*
194021, Россия, Санкт-Петербург, Политехническая ул., 26
alex.nabereznov@mail.ioffe.ru

ВАХРУШЕВ Сергей Борисович – *доктор физико-математических наук, старший научный сотрудник, заведующий лабораторией нейтронных исследований Физико-технического института им. А.Ф. Иоффе РАН, профессор кафедры физической электроники Санкт-Петербургского государственного политехнического университета.*
194021, Россия, Санкт-Петербург, Политехническая ул., 26
s.vakhrushev@mail.ioffe.ru

ФОТИАДИ Александр Эпаминондович – *доктор физико-математических наук, профессор, заведующий кафедрой физической электроники Санкт-Петербургского государственного политехнического университета.*
195251, Россия, Санкт-Петербург, Политехническая ул., 29
fotiadi@rphf.spbstu.ru

КОРОЛЕВА Екатерина Юрьевна – *кандидат физико-математических наук, старший научный сотрудник Физико-технического института им. А.Ф. Иоффе РАН, доцент кафедры физической электроники Санкт-Петербургского государственного политехнического университета.*
194021, Россия, Санкт-Петербург, Политехническая ул., 26
e.yu.koroleva@mail.ioffe.ru

ГОЛОСОВСКИЙ Игорь Викторович – *доктор физико-математических наук, ведущий научный сотрудник отделения нейтронных исследований Петербургского института ядерной физики им. Б.П. Константинова РАН.*
188300, Россия, Ленинградская область, Гатчина, Орлова Роща
golosov@mail.pnpi.spb.ru

КУМЗЕРОВ Юрий Александрович – *доктор физико-математических наук, главный научный сотрудник, заместитель директора отделения физики диэлектриков и полупроводников Физико-технического института им. А.Ф. Иоффе РАН, профессор кафедры физической электроники Санкт-Петербургского государственного политехнического университета.*

194021, Россия, Санкт-Петербург, Политехническая ул., 26

yu.kumzerov@mail.ioffe.ru

НАКЕ Бернард – *доктор инженерии, профессор, директор Института электротехники Университета Вильгельма Лейбница.*

30167, Германия, Ганновер, Вельфенгартен, 1

nacke@etp.uni-hannover.de